ANALYSIS OF MUD MOTOR STALLS AND ITS IMPACT ON PERFORMANCE IN HIGH TEMPERATURE UNCONVENTIONAL RESERVOIRS

A Thesis

by

ZACHARY IRA HOPKINS

Submitted to the Office of Graduate and Professional Studies of
Texas A&M University
in partial fulfillment of the requirements for the degree of

MASTER OF SCIENCE

Chair of Committee,	Samuel Noynaert
Committee Members,	Matthew Kuttolomadom
	Eduardo Gildin
Head of Department,	Jeff Spath

August 2018

Major Subject: Petroleum Engineering

ABSTRACT

The objective of this study was to perform analysis in to the mechanisms of motor failure in the curve lateral portion of an operators high temperature Eagleford shale wells. This was achieved through multiple high frequency downhole sensors that collected drilling dynamics and vibration data. The high frequency downhole sensors were able to provide evidence of 21 motor stalls which began in the last 1,200 ft of the lateral section.

The motor stall discussed in this paper appeared to be caused by a sudden increase in weight applied downhole, which caused the torque required to rotate the bit to exceed the torque that was supplied to the bit. The stall was only released once the string shortened from the continued top drive rotation which allowed the weight applied and subsequent indentation depth of the bit to be reduced and allow the bit to rotate. Additionally the pressure required to stall the motor was decreased as the motor experienced stalls and became damaged.

Surface measurements during the stall did not reflect the true conditions downhole due to the nature of the 1 Hz recording capability. Surface measured differential pressures were hundreds of psi below actual downhole differential pressure, and did not demonstrate the extent of the damage that the motor was seeing.

Motor damage and fatigue was correlated through the use of MSE_{bit} and pressure normalized rate of penetration (ROP). These metrics were able to provide the approximate depth of the onset of motor stalls and show the progression of performance loses throughout the lateral.

Motor stalls cannot be eliminated completely but design changes can be made to lessen the frequency, and improve motor life. Design changes including bottom hole assembly (BHA)

design, motor configurations, as well as a real-time deration practice are presented in a workflow to manage motor stalls.

ACKNOWLEDGEMENTS

I would like to thank my committee chair, Dr. Noynaert, and my committee members, Prof. of Engineering Practice Fred Dupriest, and Dr. Kuttolamadom for all their input and recommendations towards this research.

Thanks also goes to my family and friends for their continued encouragement throughout my time at Texas A&M University.

CONTRIBUTORS AND FUNDING SOURCES

This work was supported by a research committee consisting of Professor Sam F. Noynaert (advisor), Professor Fred Dupriest of the Department of Petroleum Engineering, Professor Eduardo Gildin of the Department of Petroleum Engineering, and Professor Matthew Kuttolamadom of the Department of Manufacturing and Mechanical Engineering Technology.

The graphs discussed in Section 1.3 were performed by Samba et al and were published in (2016) in a paper listed in the references section. The figure discussed in Section 1.1 was published by Cresecent Directional Drilling in 2011 and edited by Weimar in a handbook listed in the references section.

Graduate study was supported by a Graduate Assistant Research position funded by Marathon Oil.

TABLE OF CONTENTS

Page

LIST OF FIGURES

Page

1. INTRODUCTION

1.1 Problem Background

The operator involved with this project has been seeing a significant number of mud motor failures in the curve and lateral sections of their wells. Along with the increased number of failures there has also been variability in performance of the motors across their acreage. The formation of interest is the Eagleford shale, an unconventional reservoir in South Texas. The wells drilled by the operator within the last year are located within the counties of Atascosa, Live Oak, and Karne shown in **Fig. 1**. Many of the wells in the acreage are considered high temperature ranging from 290°F to 330°F.

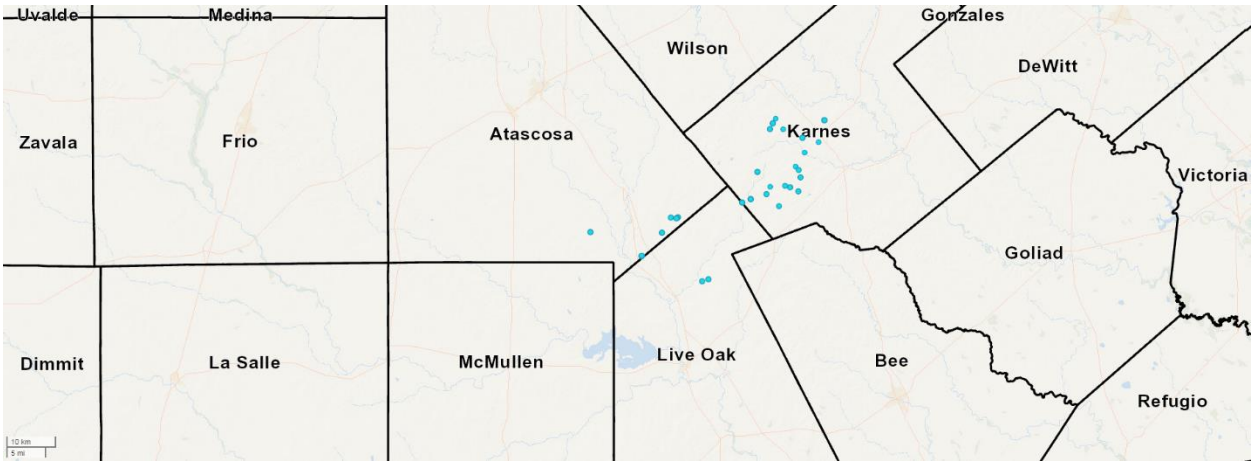

Fig. 1 - Operator drilling activity 6/17 to 6/18

The wells located in Fig. 1 total 78, and have experienced 22 motor failures with a rate of close to 30%, often times experiencing failures in the same well. The bottomhole temperatures regularly exceeded 300°F during failures but some wells did experience failures in sub 300°F

environments. The operator has progressed to motors with a larger amount of stages which has had little effect on the incidence of failure.

The high temperature encountered during drilling requires the fit of the motor to be changed and the allowable differential pressure to be de-rated (Dyck, 2011). The fit of the motor is a function of the rotor, elastomer, and stator diameter displayed in **Eq. 1**. The fit of the motor has a drastic effect on the performance and life of a mud motor (Dyck, 2011). If the fit of the motor is too loose the performance of the motor is reduced, because the rotor and elastomer will not create discrete cavities and allow fluid to flow through. If the fit of the motor is too tight then the contact pressure between the rotor and elastomer will be too high which will cause fatigue to the elastomer. The increased temperature seen in the Eagleford wells causes the elastomer to swell and tightens the fit. The motors are designed with a looser fit to account for the increased temperature.

$$Fit = (Rotor\ Major\ Diameter - Lobe\ Height) - Stator\ Minor\ Diameter \quad \ldots\ldots\ldots\ldots\ldots\ldots\ldots\ldots (1)$$

The BHA design for a majority of the operator's wells involves an unstablized BHA with a bent motor ranging in bends from 2° to 2.12°. A typical BHA configuration can be seen in **Fig. 2.** Motor configurations include power sections ranging from 6 to 11 stages, and stator rotor lobe configurations of 5/6 and 7/8.

Motor Properties

Description:		Motor Type:	Manufacturer:	Model:	Serial Number:	Lobe/Stage:
7" Motor 2.12° FBH 7/8 Lobe; 9.4 Stages		Motor				7/8/9.4
Mud Type:		Stabilizer Type:		Rubber Type:		Fit Type:
		IB		HR		-0.02
Pad OD:	NB Stabilizer:	Bit to Bend:	Bend Angle:	Pressure Drop:	Rev. Rate:	Rotor Jet:
7 9/16in	8 1/4	4.37ft	2.120°	0psi	0.29Rev/gal(US)	0/32's
Motor Footage:	Below Rotary Hours:	Circulating Hours:	Rotating Footage:	Rotating Hours:	Sliding Footage:	Sliding Hours:
0.00ft	0.00hrs	0.00hrs	0.00ft	0.00hrs	0.00ft	0.00hrs
Proposed Build Rate:	Actual Build Rate:	Date/Time In:	Date/Time Out:	Number of Stalls:	Stall Duration:	Extended Motor:
12.000°/100ft	0.000°/100ft	12/01/17 6:17 PM		0	0.00mins	No
Motor Failed:	Condition:					
No						

Bit Record

Bit Number:	Description:	Manufacturer:	Model:	Type:	Serial Number:
3	8 3/4" PDC Bit			PDC Bit	38076
IADC#:	Bit Diameter: / TFA:	Jets:		Condition:	
	8 3/4in / 2.237in²	8 x 18, 1 x 18		No Dull Characteristics	
Bit Hours:	Bit Footage:	Reason for pulling out of hole:			
0.00Hrs.	0.00ft				

Drillstring Components (Run #3 Curve/ Latera)

Item #	Description	Vendor	Serial No.	Outside Diameter (in)	Inside Diameter (in)	Linear Weight (lbs/ft)	Component Weight (lbf)	Top Connection	Length (ft)	Total Length (ft)
1	8 3/4" PDC Bit			8 3/4	2 7/8	0.00	0	4 1/2 REG	1.25	1.25
2	7" Motor 2.12° FBH 7/8 Lobe; 9.4 Stages			7	0	0.00	0	XT54	41.23	42.48
3	Float Sub			6 3/4	2 7/8	0.00	0	XT54	2.42	44.90
4	NM Pony Collar			6 3/4	3 1/2	0.00	0	XT54	9.06	53.96
5	MWD Collar			6 11/16	3 1/2	0.00	0	XT54	28.12	82.08
6	Pulser Sub			6 3/4	3 1/2	0.00	0	5 1/2 FH	4.82	86.90
7	NM Crossover			7 3/16	2 7/8	0.00	0	XT54	3.31	90.21
8	NM Flex Collar			6 3/4	3 1/2	0.00	0	XT54	29.83	120.04
9	NM Flex Collar			6 3/4	3 1/4	0.00	0	XT54	30.13	150.17
10	Filter Sub			7 1/4	2 7/8	0.00	0	HT55	5.44	155.61
11	5 1/2" DP (95 Jts)			5 1/2	0	0.00	0	HT55	2,991.55	3,147.16
12	Aggitator / Shocksub			7	2 1/2	0.00	0	HT55	26.04	3,173.20

Drillstring Discussion

Bit #3: 8 3/4" I ; Jets: 9 x18 TFA: 2.237 ; Gage Length: 4.50"
- 7" Mud Motor 2.12° FBH 7:8 Lobe; 9.4 Stages / RPG: 0.29 / BTB: 4.37`
Max Flow: 750 GPM
Max Diff: 2000 PSI
Max Torque: 18,680 FT-LBS

4R Float Valve in Float Sub

Bit to Survey: 72`
Bit to Gamma: 63`

Fig. 2 – Typical BHA design and motor configuration including 2.12° bend 7/8 lobe and 9.4 stages

1.2 Mud Motors

Mud motors are progressive cavity displacement pumps placed in the drill string which provides additional power to the bit, and when built with a bent housing for the universal joint, give the ability to directionally steer. They traditionally consist of a top sub connecting the motor to the drill string, a power section containing a rotor inside an elastomer lined stator, and a transmission section to convert the eccentric power of the motor to concentric power to the bit as

seen in **Fig. 3**. The rotor of the power section will have one fewer lobe than the stator to enable discrete amounts of fluid to be pumped and allow the rotor to rotate driving the bit.

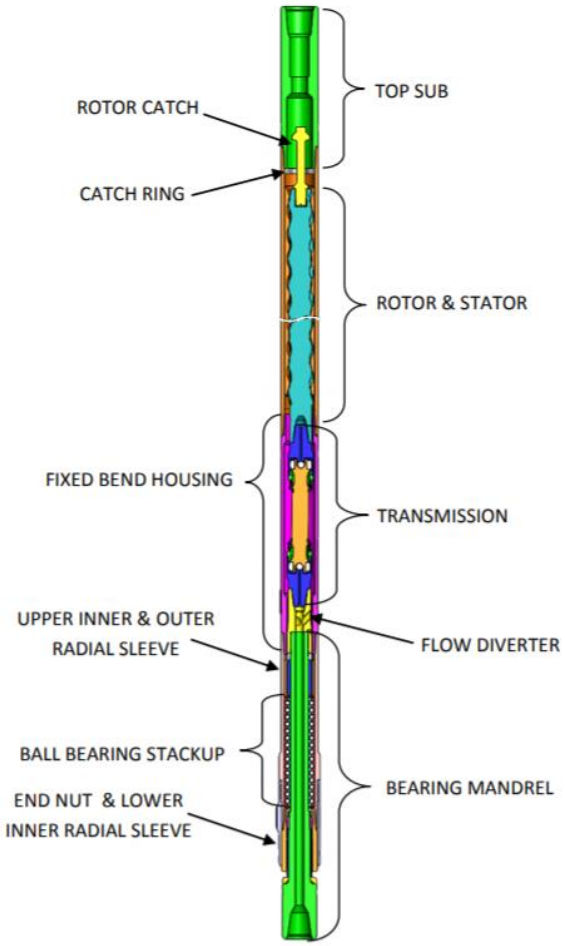

Fig. 3 – Mud motor assembly (reprinted from Weimar, 2011)

To allow the bit to steer there is a bend in the housing of the motor, which enables directional control when not rotating the string. When the string is rotated during normal drilling operation a mass imbalance is created which creates an oscillating sine wave in the BHA (Dupriest et al, 2009). This is a common cause of drilling inefficiency, known as whirl, which creates violent collisions of the bit and BHA with the borehole wall. These oscillations induce

premature tool fatigue and damage. In addition to the damage whirl provides it also increases the temperature of tools and negatively affects the elastomer within the power section.

1.3 Mud Motor Failure Mechanisms

The two most common failure mechanisms of mud motors are in the power section and the bearing assembly. Failures in the bearing assembly occur from high torque events. A bit that is experiencing full stick will create large torque events when the bit comes to a complete stop, and must torque up to break free as demonstrated by Craig et al (2010). This large torque event will create stress inside the bearing assembly and cause premature failure.

Failures in the power section can occur through debonding of the elastomer from the stator, or what is commonly called “chunking”. Elastomer debonding is a problem that involves the incompatibility of the drilling fluid and the elastomer as noted by John (1997). While common in some areas, elastomer debonding is not usually encountered in the wells this study covers. The common problem seen and studied in this work is the chunking of the elastomer.

As fluid is pumped through the motor, pressure differences within the lobes of the stator create rotation of the rotor. If the motor is operating efficiently, and the fit of the motor is designed correctly, the cavities will be sealed from one another. If the differential pressure of the motor is high enough the elastomer will deform and there will no longer be discrete cavities within the motor. A large amount of fluid flowing across the elastomer will increase erosion of the rubber, and also decrease volumetric efficiency as less fluid is rotating the rotor (Anyanwu, 2012. Samba et al, 2016). Increased differential pressure across the motor has other negative effects other than erosion and a reduction in volumetric efficiency. As the rotor turns inside of the stator, the differential pressure deforms the elastomer in a cyclic process. This cyclic loading

of the elastomer creates stress induced cracks (Samba et al, 2016). These stress cracks can propagate and may become large enough to fragment the elastomer leading to motor chunking. A motor that has been chunked can be seen in **Fig. 4** and **Fig. 5**. The elastomer will begin to fail from the lower stages of the power section towards the top, as the lower stages perform more work than the stages higher in the power section investigated by Denney et al (2012). From previous wells investigated, all motors do have some form of elastomer chunking. The severity of chunking will determine whether the motor can drill to total depth (TD) or not.

Fig. 4 – Upper stages of power section with little elastomer chunking

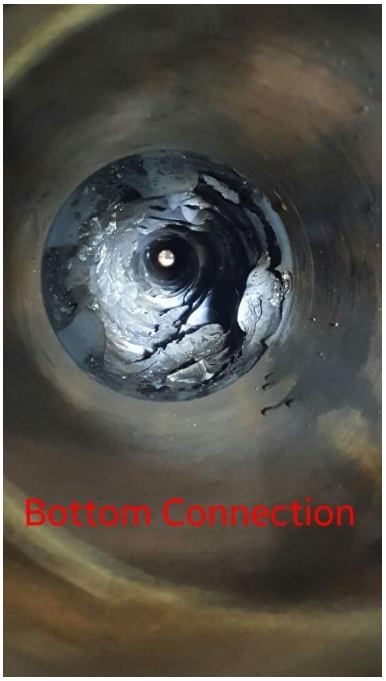

Fig. 5 – Lower stages of power section with elastomer chunking

Hysteresis heating is also a concern of high differential pressure loading. The elastomer located inside of the stator is a nonlinear material and follows a different path along the stress strain curve during loading and unloading as shown by Samba et al (2016) in his **Fig. 6**. As the rotor rotates each section of the elastomer is continuously loaded and unloaded and will see hundreds of thousands of cycles for a typical length bit run. The closed loop of the stress strain curve is known as a hysteresis loop, and the energy contained within the loop is converted to heat. Hysteresis heating is the result of the thermal energy created during the cyclic loading further evidenced by Beeh et al (2018). Therefore the higher the flowrate through the motor, and in turn the higher the RPM, the higher the temperature that will be seen within the elastomer.

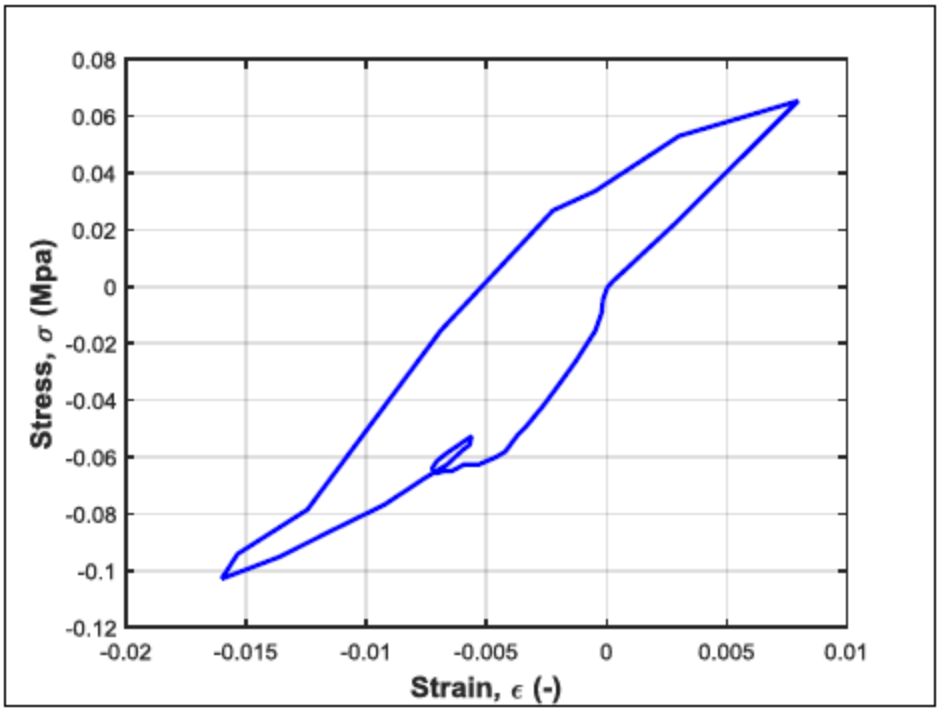

Fig. 6 – Stress strain relationship of an elastomer demonstrating material nonlinearity during loading and unloading with a closed hysteresis loop (reprinted from Samba et al, 2016)

In some instances, there is a processes of runaway heat caused by hysteresis heating seen with high differential pressure and high motor rpms further investigated by Samba et al (2016) and Beeh et al (2018). The differential pressure must be suitably high to create large strain energy which is then converted to heat during cyclic loading. As stated earlier with an increase in temperature the elastomer swells and the fit between the elastomer and rotor is tighter. This tighter interference fit enables for a higher contact pressure, and in turn further increases strain energy. This process continues and the temperature begins to run away and never stabilizes. Samba et al, (2016) demonstrates this in his **Fig. 7**. Regardless of the flowrate, the temperature within the elastomer will increase resulting from hysteresis heating and cause the elastomer to continue swelling.

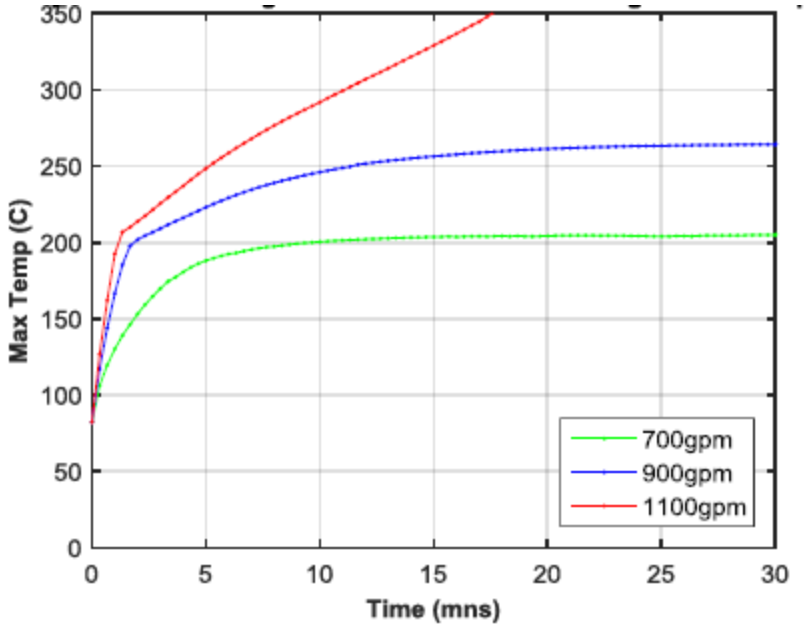

Fig. 7 – The effect of flowrate on elastomer temperature demonstrating hysteresis heating and run away heat effect (reprinted from Samba et al, 2016)

1.4 Mechanical Specific Energy

Mechanical Specific Energy or better known as MSE, is a measure of the energy used per volume of rock drilled shown by Teale (1965). MSE is used to quantify drilling efficiency and can be utilized through surveillance and forensics to determine areas of drilling inefficiency and damage occurring downhole.

$$MSE_{surface}\ (psi) = \frac{480 * Torque * RPM}{D^2 * ROP} + \frac{4 * WOB}{\pi * D^2} \quad \text{(2a)}$$

$$MSE_{bit}\ (psi) = \frac{480 * Bit\ Torque * Bit\ RPM}{D^2 * ROP} + \frac{4 * WOB}{\pi * D^2} \quad \text{(2b)}$$

Two forms of the MSE equation can be used which are $MSE_{surface}$ and MSE_{bit} shown in **Eq. 2a, and Eq. 2b**. $MSE_{surface}$ uses surface measured torque and RPM and does not accurately reflect the energy actually being expended downhole for rock cutting. The torque and drag in the system will increase significantly as the bit begins to drill the curve and into the lateral. Therefore, all of the torque measured at the surface is not being used to cut the rock; some of it is lost through drillstring-wellbore wall contact in the curve and lateral.

A more accurate measurement of the energy expended to break the rock is MSE_{bit}. This measure of MSE replaces the surface torque and RPM measurements with the theoretical amounts generated by the motor at the current operating parameters. A mud motor's performance is defined by power curves generated by the manufacturer which have a rotation and torque rating based on differential pressure and flowrate. With the flowrate and differential pressure across the motor known, the equivalent downhole torque and additional RPM can be found that is powering the bit. MSE_{bit} is a much more accurate representation, and when plotted against $MSE_{surface}$, MSE_{bit} will be the lower of the two. When plotted against each other the two curves should follow the same trends and be offset by the amount of inefficiencies in the system above the motor.

During perfectly efficient drilling, MSE_{bit} will equal the unconfined compressive strength of the rock as shown by Teale (1965). This means that that all of the energy supplied to the bit is being used to remove the rock. When used on a drilling rig, the value of MSE_{bit} does not equal the rock strength because of drilling inefficiencies or mud motor degradation. This is the reason MSE_{bit} is used in a relative sense instead of looking at the absolute numbers output by the MSE equation. In general, if the bit is drilling efficiently then ROP should increase linearly as either weight on bit (WOB) or rotation of the top drive in revolutions/min (RPM) are increased. As

long as the response is linear, the MSE will remain the same. This is because there may be more energy going into the system but there is a proportional response in ROP. If the MSE increases, then the system is drilling less efficiently than before and some form of dysfunction is now present in the system causing a nonlinear response in performance. If MSE decreases then the system is becoming more efficient, likely resulting from the reduction or elimination of a dysfunction that was present. **Fig. 8** shows the MSE response during a WOB step test.

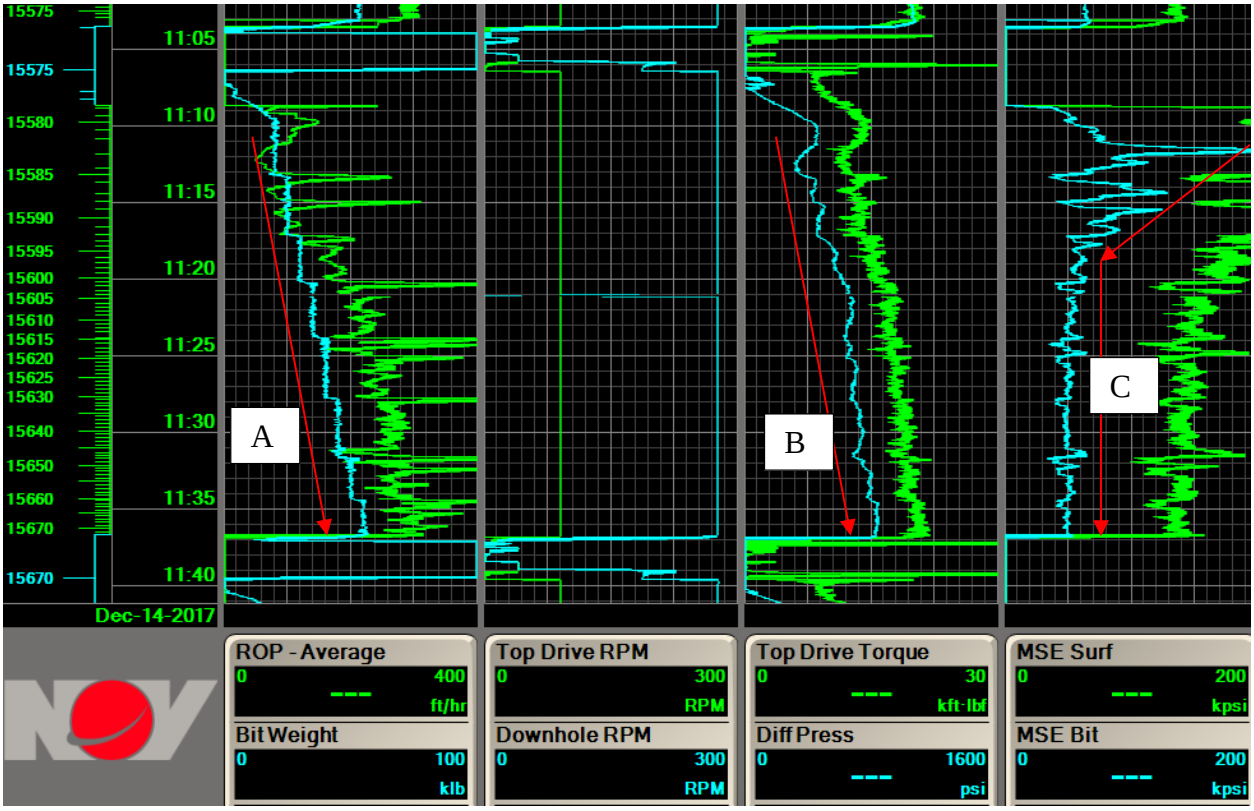

Fig. 8 – WOB raised in 5,000 lbf steps (A) as differential pressure increases (B) and the subsequent reduction in MSEbit and MSEsurface (C) as whirl is suppressed and MSEbit remains constant indicating efficient drilling.

During a step test WOB is increased in 5,000 lbf increments and the MSE_{bit} response is observed to find the WOB that has the most efficient drilling, through the blue curve on the

fourth track. When low WOB is applied the MSE_{bit} response is high because the cutters of the bit are not engaged fully and the bit is experiencing whirl (Dupriest et al, 2009). As the weight continues to increase the MSE response stays flat. This is an indication of efficient drilling and that increasing weight is not introducing any drilling inefficiency. The flat portion of the MSE_{bit} response can be used as a baseline to determine the most efficient drilling. The measure of MSE_{bit} enables it to be used to determine the presence of drilling inefficiency and also reflects on the performance of the motor.

2. FIELD TRIALS

2.1 Motor Stalls

The objective of this study was to find evidence of damaging events that impact the performance and life of a mud motor and any measure that can be taken to reduce them. To achieve this task a well was chosen to run high frequency drilling dynamic sensors in the curve and lateral section of the well. One sensor was located 7 ft above the motor measuring drillstring torque, drillstring pressure, drillstring RPM, WOB, and tri-axial accelerations. The second sensor was placed within the bit and measured tri-axial accelerations. The well investigated did not have a failure as determined by the operator, but did provide evidence of motor stalls and was found to have lost a significant portion of elastomer as determined by the motor vendor. The high frequency sensors were able to provide evidence of at least 21 motor stalls which predominantly occurred in the last 1,200 ft of the lateral.

Motor stalls are the event that is primarily investigated in this paper and causes significant damage to the power section of the mud motor. Theoretically, the torque relationship of a mud motor is linear, and as differential pressure is applied across the motor torque is produced that is supplied to the bit. Motor stalls occur when the torque required to rotate the bit exceeds torque that is supplied to the bit. Explained earlier, as the differential pressure increases the elastomer is deformed which enables the fluid to bypass the motor reducing volumetric efficiency. Once a certain differential pressure across the motor is reached there will be zero rotational output from the motor and it will effectively be stalled discussed by Anyanwu (2012). Guidroz (2011) and Alattar (2017). These events are very damaging to the motor components and occur many times during the drilling of a well.

The sensor placed above the motor recorded high frequency measurements in a two second burst window. **Fig. 9, Fig. 10, Fig. 11,** and **Fig. 12** below are of a two second burst window recorded at 04:10 a.m. at a depth of 13,415 ft roughly 2,000 ft in to the lateral containing a motor stall.

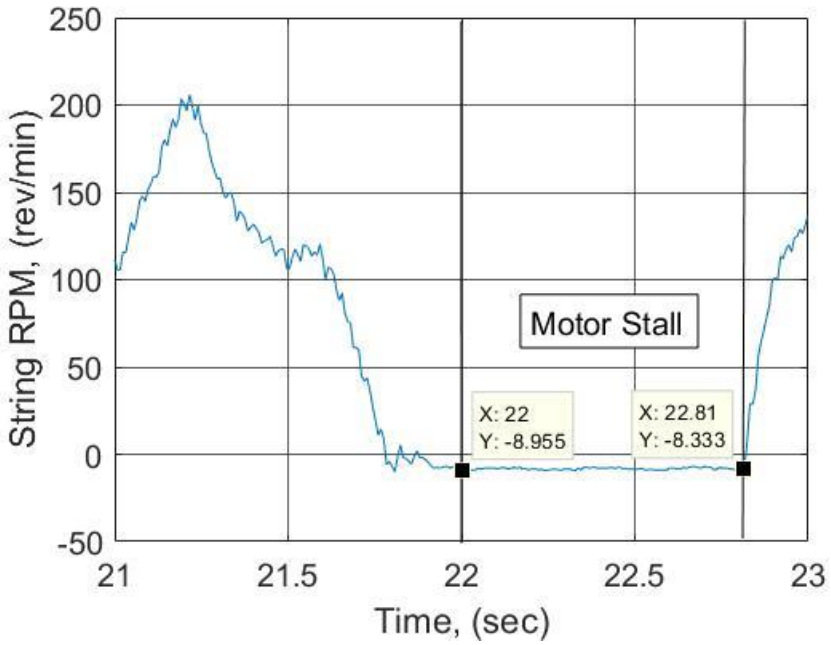

Fig. 9 – String RPM reaching zero and remaining stationary

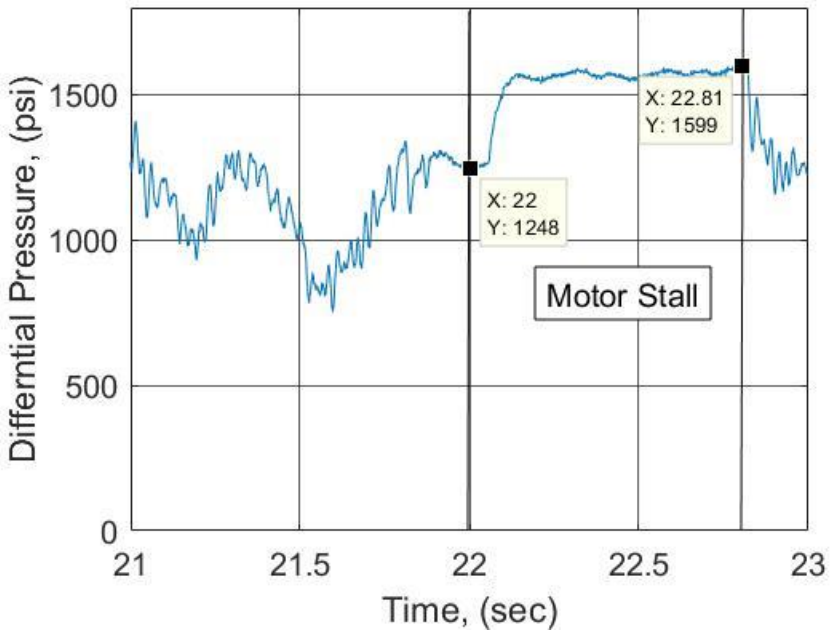

Fig. 10 – Differential pressure reaches a value suitable to stall motor

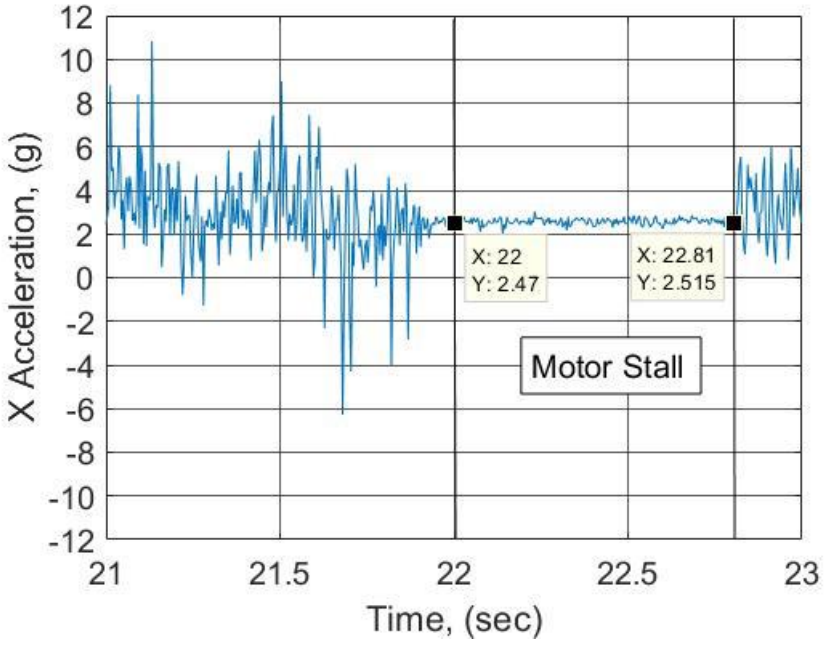

Fig. 11 – X accelerations hold constant during stall indicating the string nor the motor rotating

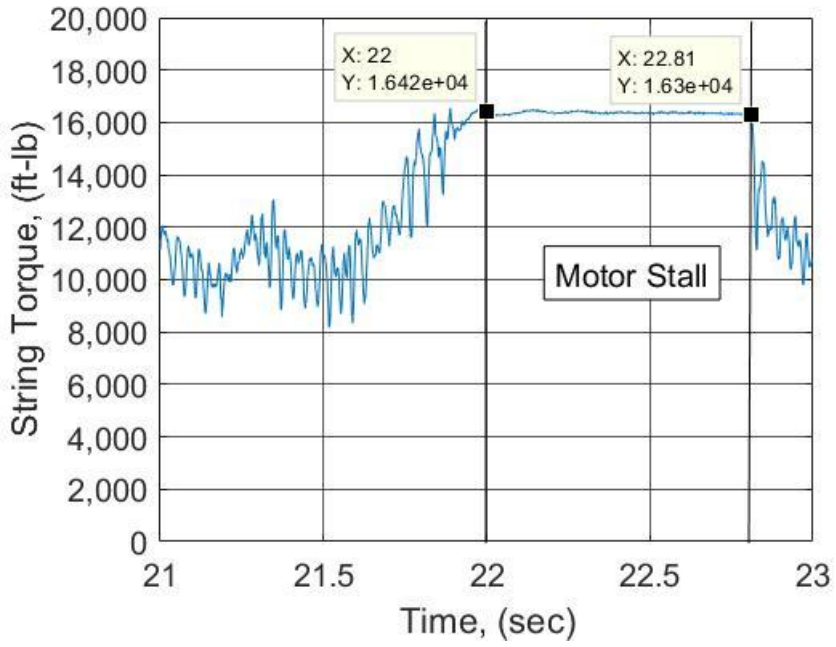

Fig. 12 – String torque peaks and remains constant as torque supplied through the motor and string is not suitable to rotate the bit

During a motor stall we expect to see the differential pressure reach a value suitable to stall the motor and stop rotation of the bit. As the differential pressure is spiking we should see the torque reach a peak and remain constant signifying the available torque the top drive and motor are able to supply. We also expect to see the string stop rotating and remain stationary as the motor is stalling and the bit is not rotating. Since the string is not rotating and the rotor of the motor is not rotating we should also expect the accelerations above the motor to flatten signifying a lack of vibration created from rotation.

The motor stalls observed were characterized by a halt in rotation of the string seen in Fig. 9. The string RPM is experiencing speed oscillation as expected and is a common occurrence seen while drilling (Dupriest et al, 2009). The speed oscillations stop and the string RPM approaches zero and comes to a complete stop. The differential pressure in Fig. 10 above

the motor is experiencing the same oscillations that the string RPM is experiencing, and then quickly climbs as the bit comes to a stop. It then reaches a peak of 1,600 psi which is well above the stall pressure of 1,100 psi as reported by the motor manufacturer. The torque in Fig. 12 also peaks to 16,000 ft-lbf and remains flat. The X accelerations seen in Fig. 11 show the string vibrating before the stall and once the stall occurs the accelerations stop and remain constant. The apparent cause of this stall can be seen as a sudden increase in weight that was applied due to weight transfer issues within the system shown in **Fig. 13**.

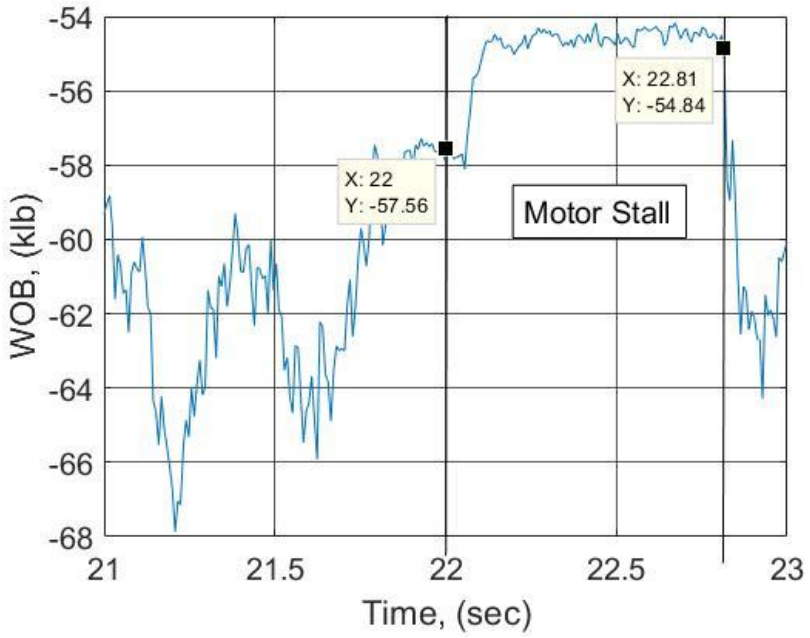

Fig. 13 – Sudden weight transfer to initiate stall and reduction in weight to release stall

The sensor readings for WOB are negative which was caused by an issue with the sensor, but the relative changes in WOB are correct. Beginning at 22 seconds a sudden increase in weight is applied which causes the motor stall. During the stall the top drive is still rotating the string and in turn is shortening it. The string has to shorten enough such that the torque required to rotate the bit reaches the value of torque supplied to the bit.

As the motor begins becoming damaged and losing elastomer we should expect the differential pressure required to stall to decrease, and stalls to become more frequent. As shown in **Fig. 14** the differential pressure during a stall 3 hours after the stall presented above has a lower differential pressure.

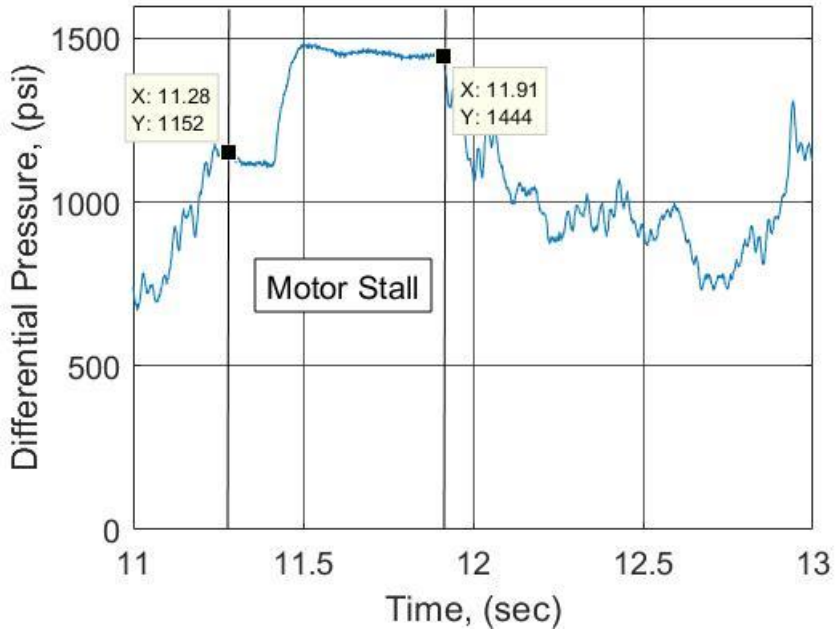

Fig. 14 – Differential pressure peaking to a value less than the previous stall

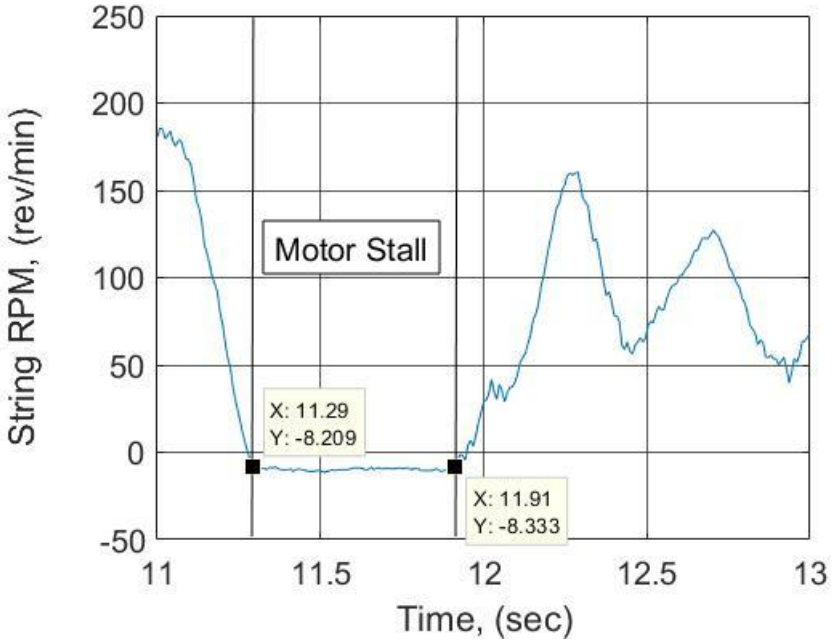

Fig. 15 – String RPM reaching zero in similar manner to first stall

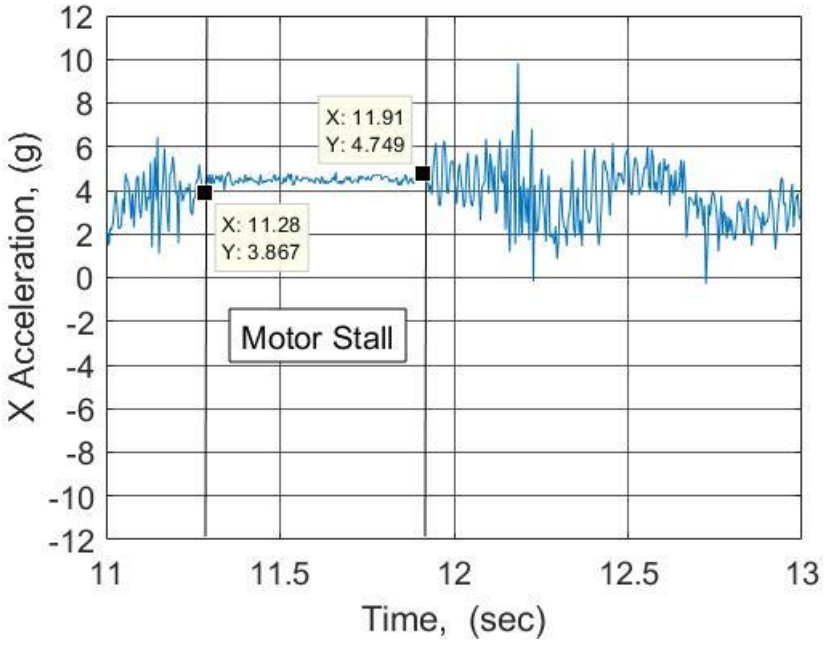

Fig. 16 - X accelerations again remain constant indication zero rotation of string and motor

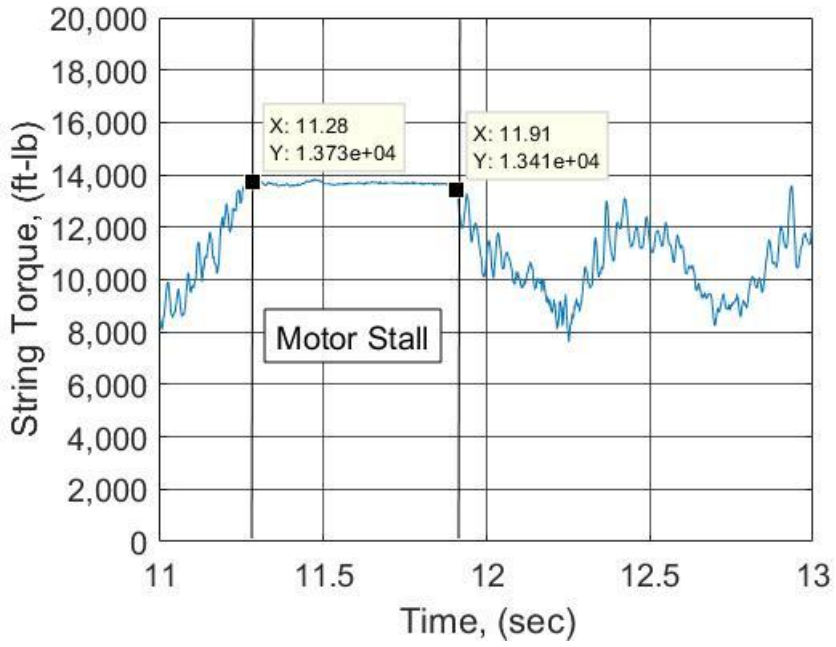

Fig. 17 – Torque reaches a peak that is less than the previous stall

The motor stall displayed in **Fig. 14**, **Fig. 15**, **Fig. 16**, and **Fig. 17** follows a similar process and shape to the previous stall. The only distinguishing feature in this stall is that the differential pressure required to stall and subsequent available torque is less. This is the cause of the frequency of motor stalls towards the end of lateral. Temperature continues to increase during drilling and as elastomer is lost the requirements to induce a stall are reduced. **Fig. 18** shows the average downhole stall pressure and surface pressure as well as the number of stalls during the last 8 hours of drilling.

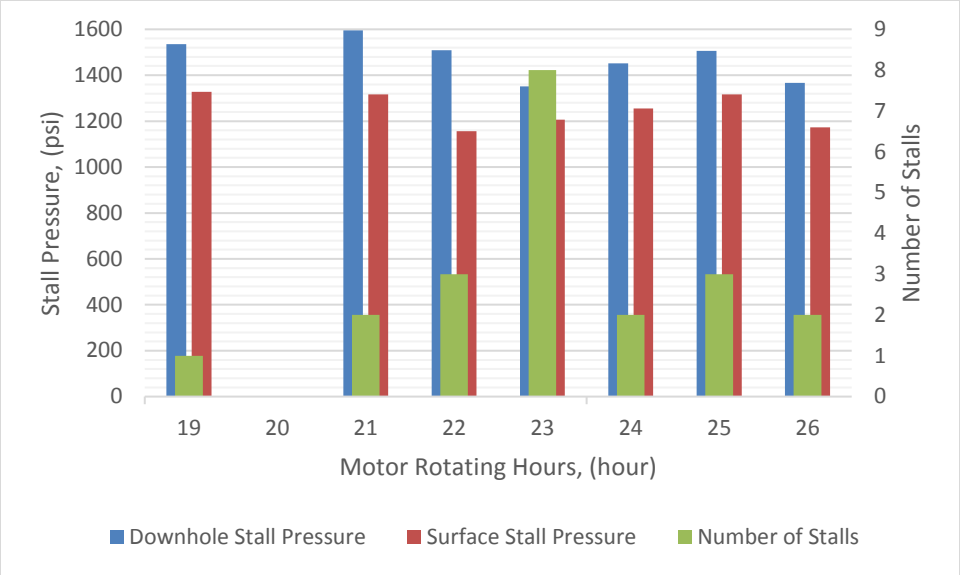

Fig. 18 – Reduction in downhole and surface stall pressure

The first four hours experienced 28% of the observed stalls and had an average downhole stall pressure of 1,546 psi. The latter four hours contained 72% of the observed stalls and the average stall pressure dropped to 1,419 psi. The 127 psi drop in average stall pressure is due to the damage the motor is incurring and the reduction of elastomer as discussed above.

2.2 Surface Detection of Motor Stalls

The difficulty with micro stalls of less than one second is being able to identify them at the surface because of the 1 Hz recording rate. One minute of WOB and differential pressure surface measurements recorded during the stall referenced in Figs. 9, 10, 11, and 12 is shown below in **Fig. 19**.

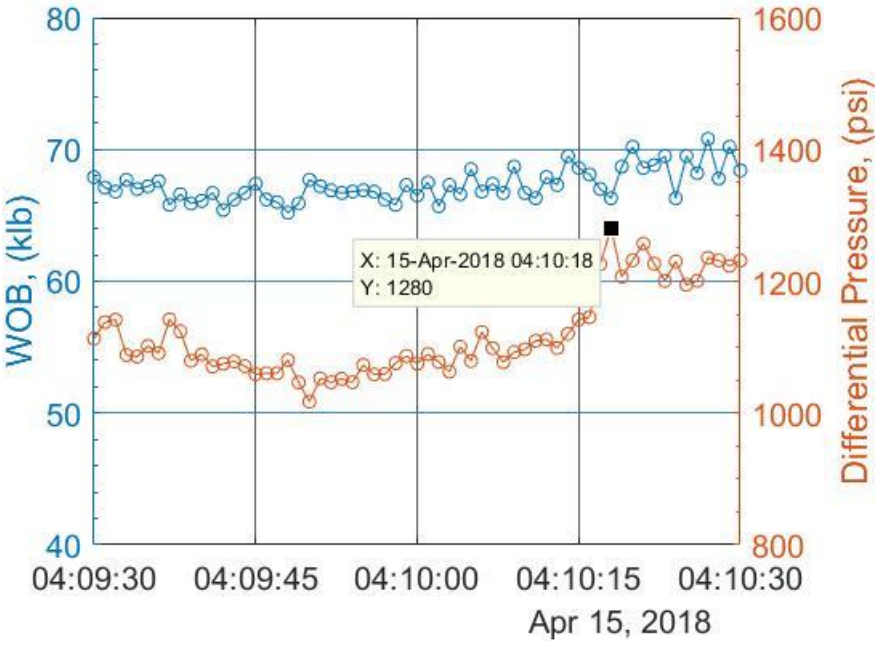

Fig. 19 – WOB drops as differential pressure peaks at 1280 psi

Surface measurements of the stall will be slightly behind the downhole measurements because of the time it takes for the pressure pulse and torque to reach the motor. The only indication that a stall may have occurred during this time is the differential pressure spike at 4:10:18. The 1600 psi differential pressure seen above the motor is not able to be seen at the surface. The erratic WOB before the observed stall at the surface could be an indication of weight transfer issues that ultimately caused the stall. The accelerations created by the varying WOB could allow the string to be released from something it is hanging up on and create the sudden jump seen Fig. 13. As stated previously the rated stall differential pressure for this motor is 1,100 psi and during drilling the motor was operating at or slightly above that value. As the differential pressure peaks it may not necessarily be cause for alarm as motors are routinely operated above their operating conditions all of the time. In reality the motor may be seeing significantly higher pressure that cannot be seen at the surface.

2.3 Motor Fatigue

With the difficulty of detecting motor stalls at the surface is there another measure we can use to quantify motor damage? Determining damage of a mud motor is a difficult task and is only determined when a drop in ROP is noticed along with rubber coming across the shale shakers. MSE_{bit} has already been demonstrated to quantify drilling efficiency, which also encompasses the performance of the motor. If the motor begins to lose elastomer and in turn loses performance, we should be able to see this reflected in the the MSE_{bit} response, if the formation has not changed and the bit is undamaged. An increase in MSE_{bit} response could result from damage to the motor or damage to the bit. This creates a difficult situation in trying to determine whether damage to the motor or to the bit is driving increases in MSE_{bit}. If drilling inefficiencies are managed and whirl is suppressed as much as possible then it can be safe to assume that the majority of the increase to MSE_{bit} can be contributed to the degrading motor performance. In this instance, the well studied did not have significant bit damage that would throw this analysis off. If the motor has been damaged, for a given WOB and theoretical bit torque we will be drilling slower than previously which would create a higher response in $MSE_{bit.}$

A simple way to perform this analysis is to observe the MSE_{bit} response over a stand while drilling the lateral. The MSE_{bit} response will have a baseline value for that stand which you can compare with stands deeper in the lateral, if drilling inefficiencies have not changed and the formation is the same. One stand of drilling at a depth of 11,258 ft at the beginning of the lateral is displayed in **Fig. 20**.

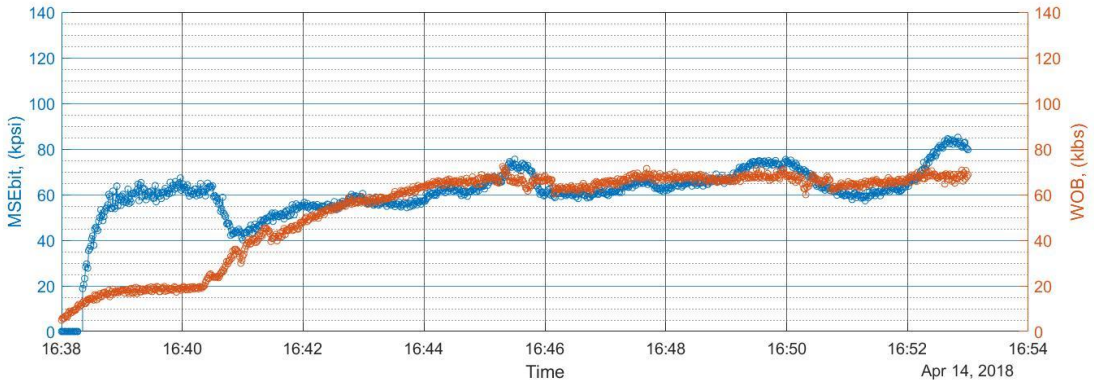

Fig. 20 – MSEbit response at the beginning of lateral showing baseline response

We can see that as we drill with 70,000 lbf WOB we are seeing an MSE_{bit} response ranging from 60,000 to 80,000 psi. As long as we are actively managing drilling inefficiencies and trying to keep the MSE_{bit} low we can use this value as the benchmark of motor performance using our current drilling parameters. We can make this same plot of a stand to see our baseline MSE_{bit} response further along the lateral. **Fig. 21** is from a depth of 14,180 ft, 2,922 ft from the previous stand.

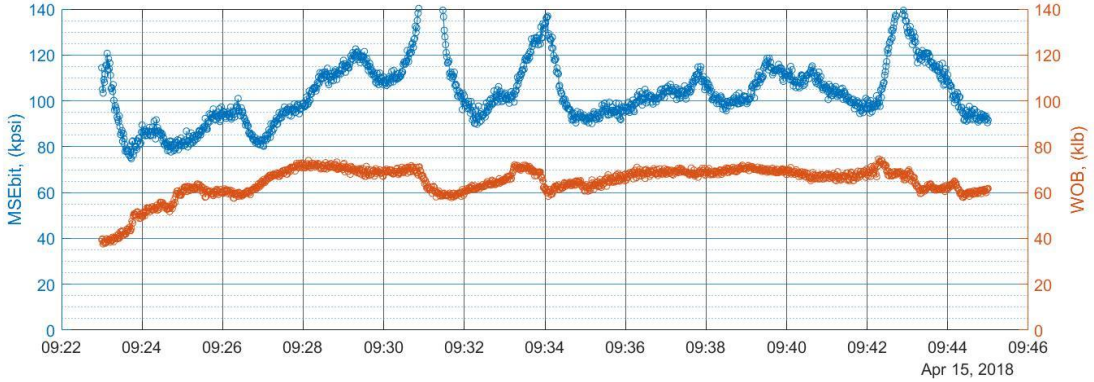

Fig. 21 – MSEbit response near the end of the lateral with higher baseline response

In this stand we are drilling with a similar WOB as with the previous stand ranging between 60,000 and 70,000 lbf WOB. We should expect to see the same baseline response as in

Fig. 20 if the motor has not been damaged and barring any changes in rock strength and drilling inefficiencies present. In this instance we see a much higher MSE_{bit} response, ranging from 90,000 psi to 140,000 psi. Step tests performed further in the lateral show that the overall inefficiency in the system has not changed much and that these plots demonstrate that the motor has been damaged and is not producing the same torque and rotation that it once was. The MSE_{bit} response naturally increases in the lateral due to weight transfer issues, but because the well has a shorter than average lateral length this issue should not create the significant change as shown in Fig. 20 and Fig. 21.

Another technique involves grouping the lateral in to sections and viewing the MSE_{bit} response over a discrete time period through histograms. The length of the lateral was grouped in to 3 hour sections and plotted using histograms with bins ranging from 40,000 to 100,000 psi. If the whole lateral was drilled with an undamaged motor and no changes in rock strength and drilling inefficiencies, we would expect to see the majority of measurements falling in to the 40,000 – 60,000 psi and 60,000-80,000 psi bin. The histograms containing 3 hours of drilling from the beginning of the lateral to TD are presented below in **Fig. 22**, **Fig. 23**, **Fig. 24**, and **Fig. 25**.

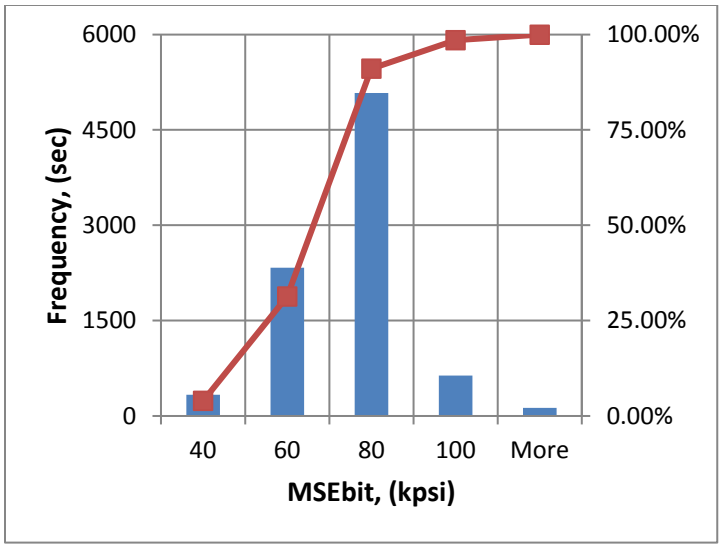

Fig. 22 – Majority of MSEbit is less than 80,000 psi as expected

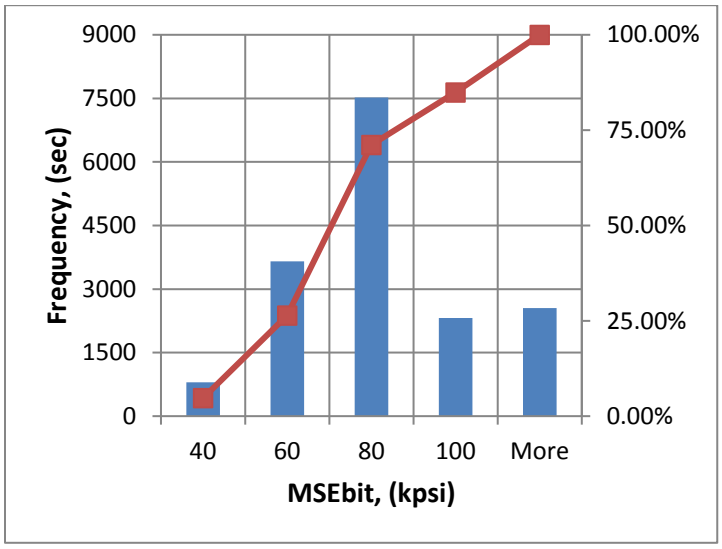

Fig. 23 – MSEbit increases over the next 3 hours of drilling as motor is damaged

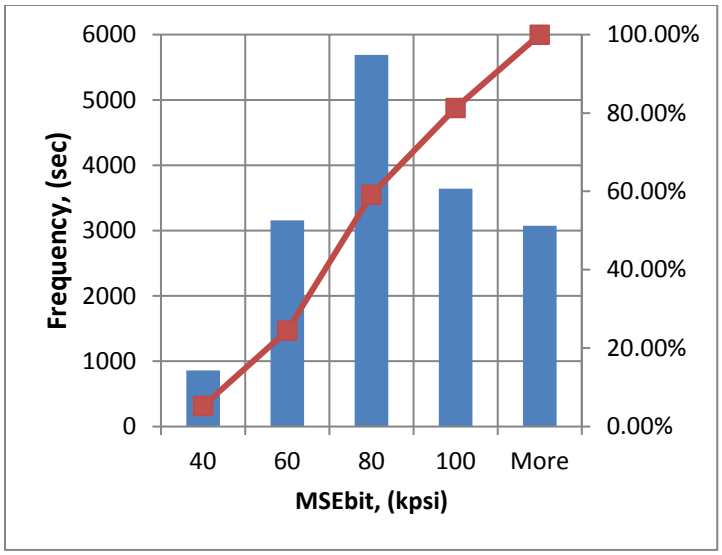

Fig. 24 – MSEbit continues increasing as motor damage accumulates

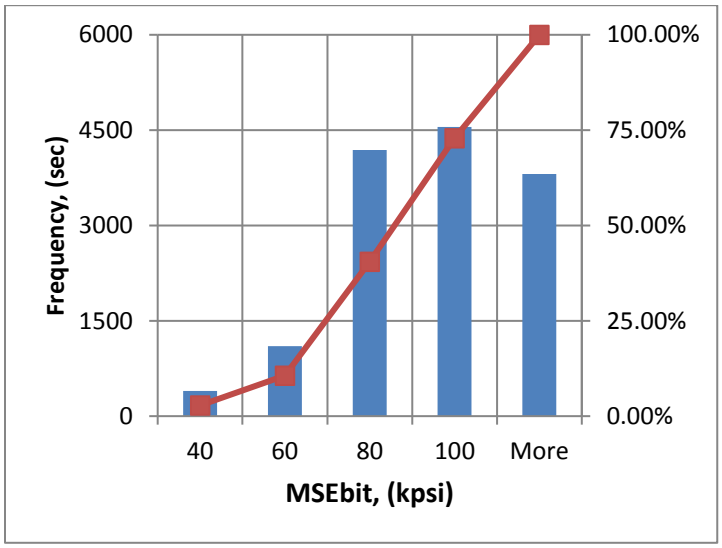

Fig. 25 – Over 50% of drilling in the last 3 hours is above our baseline response in the lateral

These figures illustrate that as drilling is continued in the lateral the MSE_{bit} response continues increasing. During the last 3 hours of drilling over one and half hours has an MSE_{bit} response greater than 80,000 psi. In contrast to the first 3 hours of drilling the lateral where only 16 minutes of drilling had an MSE_{bit} response greater than 80,000 psi.

ROP can also be normalized by differential pressure and plotted alongside MSE_{bit} in 100 ft averages to determine the approximate depth that the stalls begin to occur. **Fig. 26** shows the point at which the stalls began to occur and the reduction in ROP per 100 psi differential pressure applied to the motor.

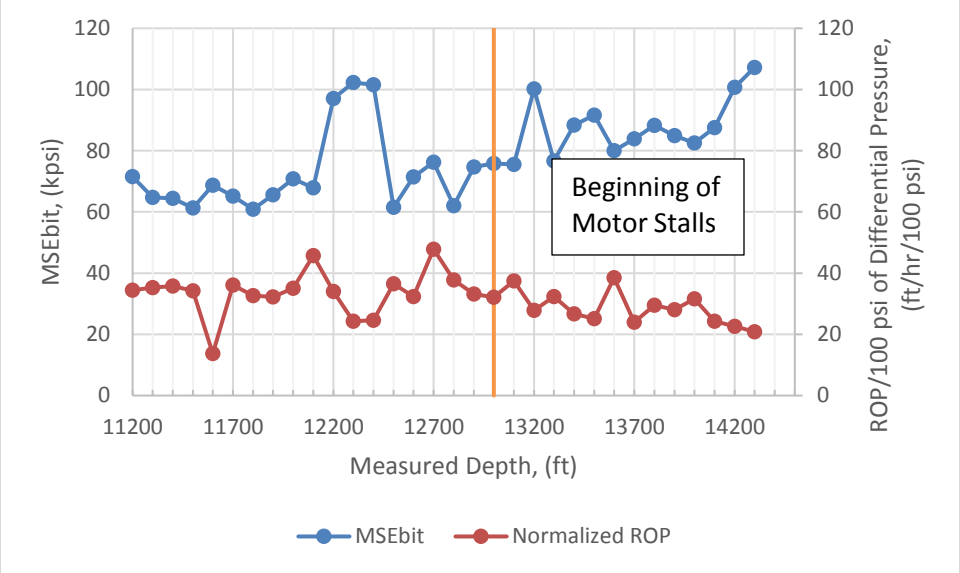

Fig. 26 – The slope of pressure normalized ROP becomes is flat before the stalls and becomes negative once the stalls begin

At the beginning of the lateral section the normalized ROP is fairly constant and does not appear to trend down. At approximately 13,000 ft measured depth, the stalls begin and the slope of pressure normalized ROP begins to become negative indicating damage.

This same motor design was run on another well and the motor became damaged to the point that it had to be replaced. **Fig. 27** is a plot of pressure normalized ROP as well as MSE_{bit} in 100 foot averages.

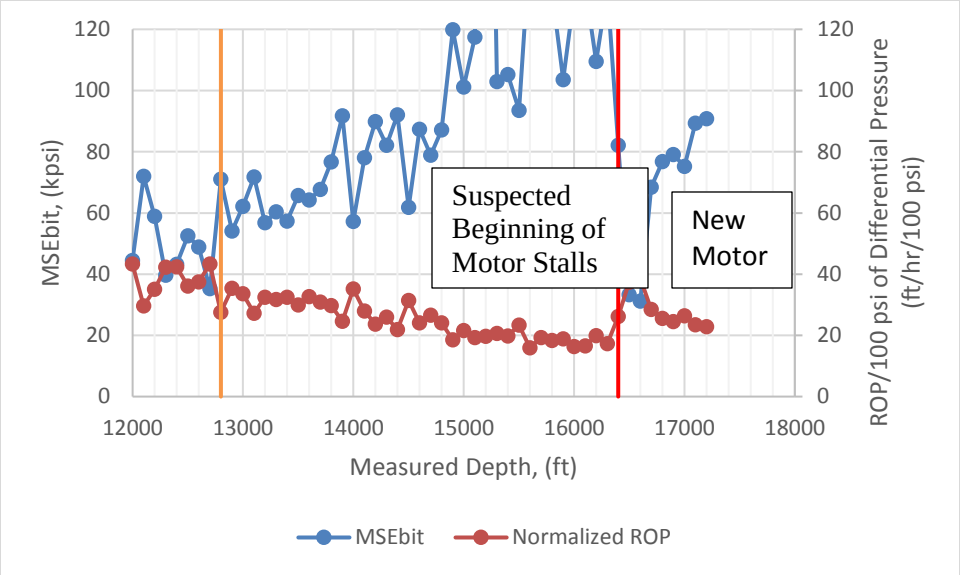

Fig. 27 – Suspected start of motor stalls occurring at 12,800 ft and increased in performance when motor was replaced at 16,400 ft.

Following the same logic as on the previous well, once motor stalls begin to occur, pressure normalized ROP should begin to drop. This places the suspected beginning of stalls occurring at 12,800 ft, at which point performance degrades until the motor had to be replaced at 16,300 ft. Once the motor was replaced the pressure normalized ROP and MSE_{bit} values improved significantly because the motor is undamaged, but then quickly begin to degrade within 300 feet indicating that motor stalls are once again occurring. Using this approach to find the approximate depth that motor stalls begin occurring, allows operating parameters to be reduced to reduce the frequency of stalls and prolong life of the motor.

3. DESIGN CHANGES

As discussed previously temperature is harmful to the elastomer of the motor causing it to swell and increasing the contact pressure between itself and the rotor. Increased temperature requires the fit of the motor to be changed and subsequently derated to a lower operating differential pressure. Currently there is not a practice implemented to continuously derate the motor operating parameters during drilling as the temperature of the motor heats up and damage occurs. We know that motor stalls cannot be eliminated completely but what we can do is reduce the temperature of the motor, and subsequently increase the pressure required to stall the motor. A previous well was investigated with high frequency sensors located in the bit which showed the extent of the temperature differences during rotating and sliding. As discussed earlier, when rotating a bent motor a mass imbalance is present that creates vibration within the BHA. The violent oscillations of the string create heat which raises the temperature. During sliding the string is not being rotated and the bit is only being driven by the motor. This eliminates the whirl that was present during rotation and will enable the bit and other tools to cool down as shown in **Fig. 28.**

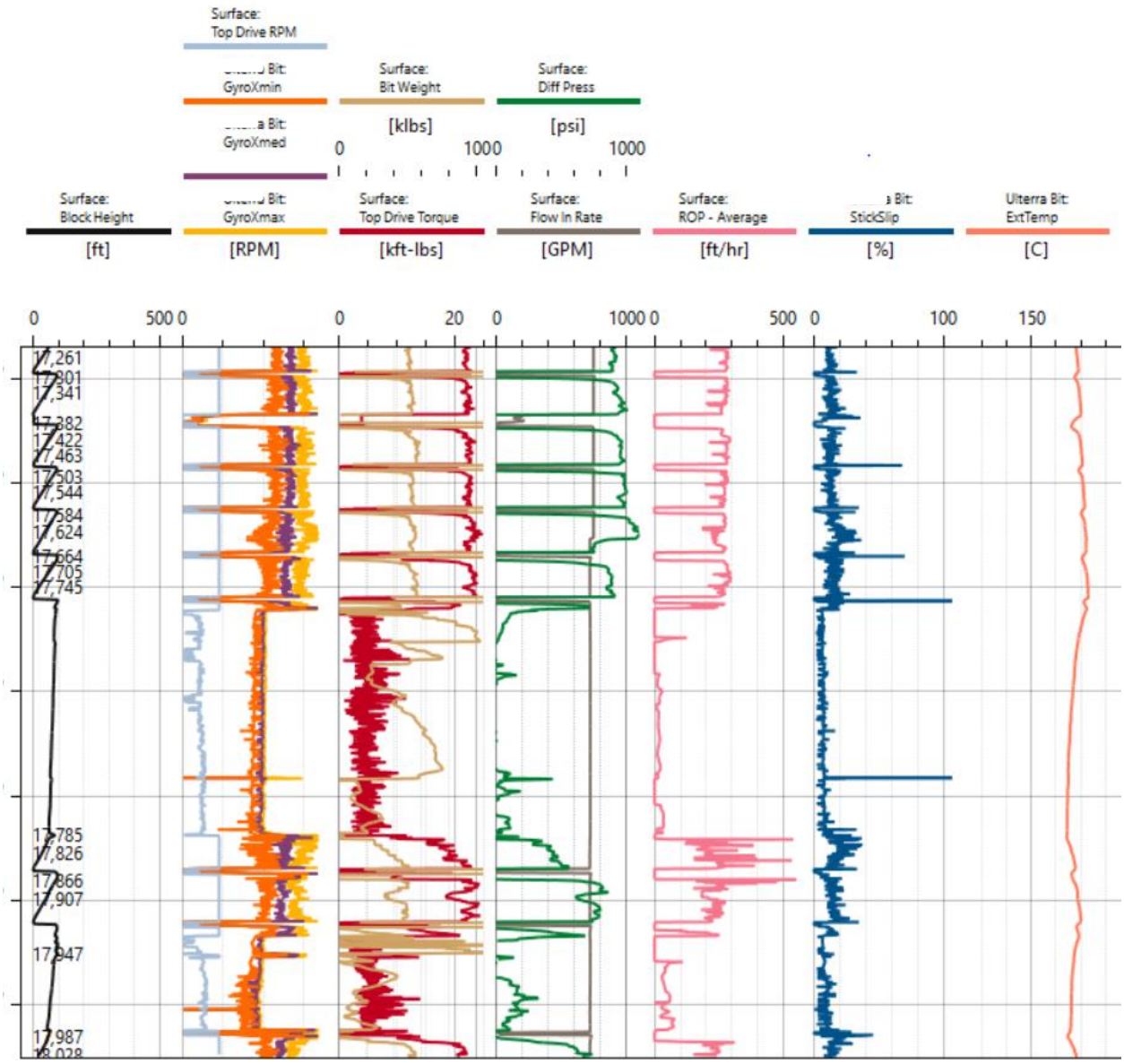

Fig. 28 – Bit external temperature cools down during slide from 17,745 to 17,785 ft

This sensor was located within the bit and not located near the motor, but the motor will be experiencing the same cooling down and heating up during slides and rotations, just at a lower temperature as it is further up the string. The slide occurs between 17,745 and 17,785 ft demonstrating the cooling down of the bit during periods of no rotation. The bit cooled down

roughly 14°F which may not seem like much, but when temperature is 300°F plus, a small reduction in temperature can have a big effect on motor damage and stalls.

Fig. 29 is the lateral accelerations from the well containing motor stalls and demonstrates the constant vibration that is experienced downhole during rotation.

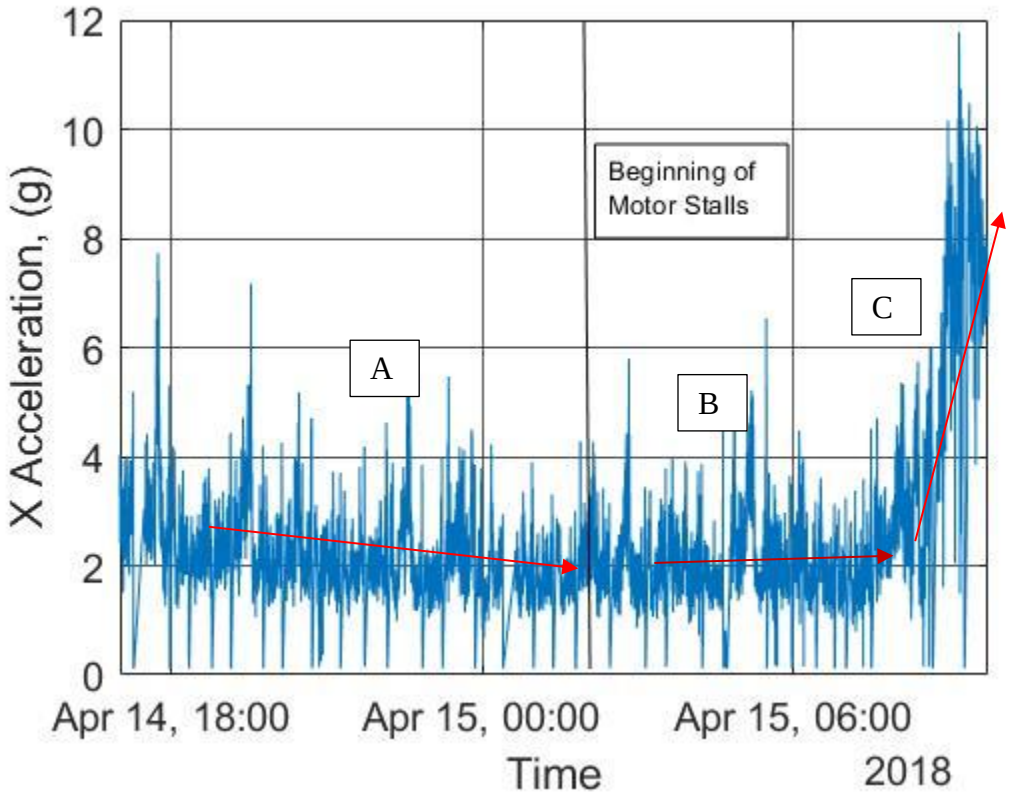

Fig. 29 – Accelerations remain constant before beginning of stalls (A) and slightly increase after stalls begin (B) until quickly climbing towards the end of the lateral (C)

Constant two g vibrations are experienced downhole during periods of rotation. This further demonstrates the violent collisions that are occurring during periods of rotation and why the temperature rises so much during rotation and cools down while there is no rotation. The vibrations also increase once the motor becomes significantly damaged. This further increases the heat generation and reduces the requirements to stall the motor.

Knowing the temperature differences seen downhole during sliding versus rotating means ideally we would want to drill the entire lateral sliding to keep temperature as low as possible and prolong the life of tools, but this isn't feasible. What can be done is trying to lessen the magnitude of the vibrations that are seen during rotation. Using a stabilized assembly the oscillating sine wave can be constrained which lessens the impact of vibrations, and reduces te temperature the motor experiences. Work performed by Bailey (2010), Craig (2010) and Bybee (2008) demonstrates that a stabilized BHA can greatly reduce the magnitude of the vibrations experienced downhole.

Another simple approach to combat the effect of the temperature generated through downhole vibrations while rotating is lowering the bend angle of the motor. A lower bend angle motor will oscillate at a lower magnitude and will reduce the impact forces the motor experiences and the heat generated. Bybee et al (2010) demonstrated this by showing the increased running time of motors with lower bend angles. Oftentimes motor designs will be selected which have higher than needed bend angles because they are drilled slick without any stabilizers, which produces a directionally unpredictable assembly. A stabilized BHA will drill predictably and will not need as high of a bend angle in the motor (Dupriest, 2009).

Lastly to combat motor stalls depth of cut control (DOCC) can be implemented behind the cutters of the bit. DOCC reduces the aggressiveness of the bit at a certain indentation depth of the cutters of the bit (Detournay et al, 1992). Once a certain weight is applied to the cutters of the bit, the DOCC behind the cutters will indent in to the surface of the rock. Once the DOCC is indented the contact area between the bit and rock is increased, but only the cutters themselves are performing the work of breaking the rock. This allows the bit to perform as designed until the DOCC are engaged, at which point it becomes less aggressive. This would solve the issues of a

sudden increase in weight that stalls the motor. This same increase in weight would not need as much torque to rotate with DOCC implemented.

Finally a real-time practice that can be used is the deration of the motors operating conditions when a decline in motor performance is observed. Using running 100 ft averages of MSE_{bit} and pressure normalized ROP shown in Fig. 26 and, Fig. 27 the depth of significant motor damage can be seen. Once the slope of pressure normalized ROP begins trending negative and the slope of MSE_{bit} begins trending positive, the operating parameters of the motor should be reduced to slow the damage of the motor. The suggested workflow involving all of the proposed design changes and real-time practices is presented in **Fig. 30.**

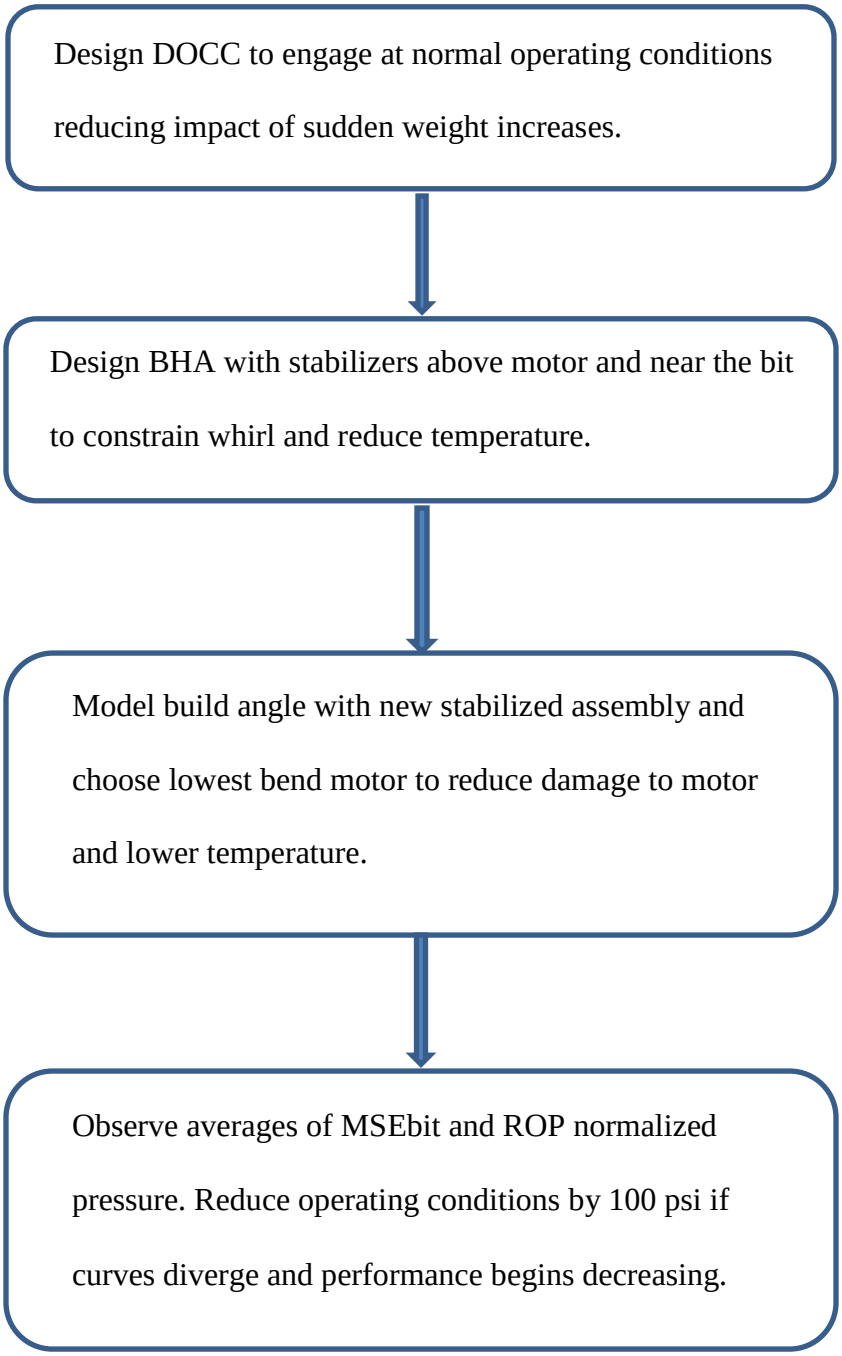

Fig. 30 – Proposed workflow to mitigate motor stalls

4. CONCLUSIONS

High frequency downhole sensors were run in an attempt to find evidence of damaging events that impact the performance of a mud motor. The operator themselves has chosen to move towards higher stage motors to combat the issue but has not seen significant success. Adding additional stages to motor is a band aid fix and will not necessarily reduce the rate of failure if the main causes of damage are not mitigated.

The burst capability of the sensors were able to capture motor stalls upwards of one second. The stalls were characterized by a sharp drop in rotation by the string, a spike in differential pressure and torque, as well as the elimination of vibrations above the motor. The stall investigated in Figs. 9 through 12 appeared to be caused by a sudden increase in weight applied downhole. This sudden weight transfer caused the cutters of the bit to indent to a point where the torque required to rotate the bit exceeded the torque being supplied to the bit. This stall was only released when the string shortened enough from the top drive rotation to allow the weight applied downhole to be reduced enough to begin rotating the bit.

The stalls only began in the last 1,200 ft of the lateral after 19 hours of drilling and within 8 hours of reaching the TD of the well. Of the last 8 hours of drilling the first four had an average stall pressure of 1,549 psi and the last four hours had an average stall pressure of 1,419 psi. This reduction in stall pressure is due to the damage the motor is experiencing, the increasing temperature of the motor.

Surface measurements during the stall period were examined and only appeared as a differential pressure spike of 1,280 psi which was 320 psi less than the differential pressure across the motor at downhole conditions. The nature of surface measurements being recorded at 1 Hz makes it difficult to see the full effect of the stall if it is less than one second.

Metrics for determining motor damage were investigated and MSE_{bit} was shown to be a reliable tool to gauge the performance of the motor if drilling inefficiencies are managed and the formation is not changing. Pressure normalized ROP can also be used to gauge the damage of the motor, and when plotted along with MSE_{bit} can show the approximate depth where motor stalls began occurring and the loss of performance began.

Lastly design changes were proposed including: DOCC, stabilized BHAs, lower bend angle motors, and a continuous motor deration based on MSE_{bit} and pressure normalized ROP. A workflow centered on these changes and practices was also introduced with the intention of reducing the aggressiveness of the bit at high WOB through DOCC, reducing the overall temperature the motor is experiencing through stabilizers and lower bend angles, and finally reducing the operating conditions of the motor once damage is observed. All the steps in the workflow work together to increase drilling efficiency and limit the damage to the motor as much as possible leading to a longer life of the motor.

REFERENCES

Alattar, A. Mustafa, M. Applegate, N.R. et al. 2017. New Positive Displacement Motor Technology Significantly Improves the Drilling Performance through Challenging and Abrasive Strata in Northern Kuwait. Paper SPE 188937 presented at the Abu Dhabi International Petroleum Exhibition and Conference held in Abu Dhabi, UAE, 13-16 November. http://dx.doi.org/10.2118/188937-MS

Anyanwu, O. N. Klotz, C. Labrecque, D. et al. 2012. Optimized Downhole Mud Motor Delivers Outstanding Performance Improvement in Alaska Coiled Tubing Drilling. Paper SPE 153474 presented at the SPE/ICoTA Coiled Tubing & Well Intervention Conference & Exhibition held in the Woodlands, Texas, 27-29 March. http://dx.doi.org/10.2118/153474-MS

Bailey, J.R. and Remmert, S.M. 2010. Managing Drilling Vibrations Through BHA Design Optimization. *SPE Drilling and Completion* **25**. 458-471. SPE-139426-PA. http://dx.doi.org/10.2118/1210-0087-JPT

Beeh, H.A. Nobre, D. Ba, S. Yan, X. et al. 2018. Drilling a Challenging Kviteborn Field 5 ¾ in. Section in a Single Run Using a New Mud Motor Modeling Engineering Workflow and New Long-Life Elastomer. Paper SPE-191331-MS presented at the SPE Norway One Day Seminar held in Bergen, Norway, 18 April. http://dx.doi.org/10.2118/191331-MS

Bybee, K. 2010. The Performance of Mud Motors With Two Different Bent Housings. *Journal of Petroleum Technology* **62.** 84-86. SPE-1210-0084-JPT. http://dx.doi.org/10.2118/1210-0084-JPT

Bybee, K. 2008. Drilling Vibrations Modeling and Field Validation. *Journal of Petroleum Technology* **60**. 73-75. SPE-1208-0073-JPT. http://dx.doi.org/10.2118/1208-0073-JPT

Craig, A.D. Goodship, R. and Shearer, D.R. 2010. High Frequency Downhole Dynamic Measurements Provide Greater Understanding of Drilling Vibration in Performance Motor Assemblies. Paper SPE 128211 presented at the IADC/SPE Drilling Conference and Exhibition held in New Orleans, Louisiana, 2-4 February. http://dx.doi.org/10.2118/128211-MS

Denney, D. Pressure Distribution in Progressing-Cavity Pumps: Performance and Run Life. *Journal Of Petroleum Technology* **64**. 85-87. SPE-0712-0085-JPT. http://dx.doi.org/10.2118/0712-0085-JPT

Detournay, E. and Defourny, P. 1992. A Phenomenological Model for the Drilling Action of Drag Bits. Oil & Gas Facilities 29(1): 13-23. http://dx.doi.org/10.1016/0148-9062(92)91041-3

Dupriest, F.E. and Sowers, S.F. 2009. Maintaining Steerability While Extending Gauge Length to Manage Whirl. Paper SPE 119625 presented at the SPE/IADC Drilling Conference and Exhibition held in Amsterdam, The Netherlands, 17-19 March. http://dx.doi.org/10.2118/119625-PA

Dyck, T. ed. 2011. National Oilwell Varco Motor Handbook, 32-42.

Guidroz, B. Barton, S. and Hussain, M. 2011. Can You Protect Your Motor Without Sacrificing Performance? Paper SPE 146575 presented at the SPE Annual Technical Conference and Exhibition Held in Denver, Colorado 30 October – 2 November. http://dx.doi.org/10.2118/146576-MS

Samba, BA, Pushkarev, M, Kolyshkin, A. et al. 2016. Positive Displacement Motor Modeling: Skyrocketing the Way We Design, Select, and Operate Mud Motors. Paper SPE 183298-MS presented at the Abu Dhabi International Petroleum Exhibition and Conference, Abu Dhabi, UAE, 7-10 December. http://dx.doi.org/10.2118/183298-MS

Teale, R. 1965. The Concept of Specific Energy in Rock Drilling. *Intl. J. Rock Mech. Mining Sci.* **2.** 57-73. http://dx.doi.org/10.1016/0148-9062(65)90022-7

Weimar, B. ed 2011. Crescent Directional Drilling Motor Handbook, 8.